International Journal of Computational Fluid Dynamics
Vol. 23, No. 10, December 2009, 723–735

Taylor & Francis
Taylor & Francis Group

Adaptive multi-resolution central-upwind schemes for systems of conservation laws

Mohammed M. Babatin[a] and Yousef H. Zahran[b]*

[a]*College of Science, Mathematics Department, Al-Imam Muhammad Ibn Saud Islamic University, Kingdom of Saudi Arabia;*
[b]*Faculty of Engineering, Physics and Mathematics Department, Port Said, Suez Canal University, Egypt*

(*Received 28 February 2008; final version received 3 March 2010*)

In this article, we develop an adaptive scheme for solving systems of hyperbolic conservation laws. In this scheme nonlinear shock and linear contact waves will be treated differently. The proposed scheme uses the Kurganov central-upwind scheme. Fourth-order non-oscillatory reconstruction is employed near shock only while the unlimited fifth-order reconstruction is used for smooth regions and linear contact waves. To distinguish between the smooth parts and discontinuities, we use an efficient adaptive multi-resolution technique. The advantages of the scheme are high resolution and computationally efficient since limiters are used only for shocks. Numerical experiments with one- and two-dimensional problems are presented which show the robustness of the proposed scheme.

Keywords: adaptive schemes; conservation laws; Euler equations; non-oscillatory scheme; central-upwind schemes; multi-resolution

1. Introduction

This article is concerned with the numerical solution of hyperbolic conservation laws. It is well known that the solutions of such systems may develop discontinuities even for infinitely smooth initial data. This makes developing high resolution non-oscillatory numerical methods for these systems a very challenging task. Here, we focus on Godunov-type projection-evolution methods, in which a piecewise polynomial interpolant is first reconstructed from the cell averages, computed at some time level and is then evolved to the next time level. There are essentially two types of this method, the simplest of which utilises a symmetric stencil and does not explicitly make use of propagation information, giving rise to central Godunov-type schemes. The second type uses wave propagation information contained in the differential equations. This is done through the solution of the Riemann problem (RP). These methods are called upwind Godunov-type methods. High-order Godunov-type schemes, both upwind and central ones, achieve high resolution with the help of high-order piecewise polynomial reconstructions. However, such reconstructions produce oscillations near discontinuities. To prevent these oscillations, limiters are widely used in the computation of polynomial pieces.

Although these limiters help to prevent oscillations near discontinuities, they are not needed, or even not desired, in smooth solutions regions because they reduce the efficiency of the method and may also cause a loss of resolution, for more details see Constantin and Kurganov (2006) and Karni *et al*. (2002). This leads to the idea of scheme adaptation. Karni *et al*. (2002) and Karni and Kurganov (2005) have presented an adaptive scheme. It is based on central-upwind scheme introduced by Kurganov *et al*. (2001) which is simple, universal and efficient for solving hyperbolic systems of conservation laws. The scheme used second-order non-oscillatory (with limiters) reconstruction near discontinuities (shocks and contact waves) and unlimited (without limiters) second-order reconstruction in smooth parts.

The motivation of this article is to develop an improved version of the adaptive scheme (Karni *et al*. 2002). The improvements are threefold. Firstly, we propose to use the fourth-order non-oscillatory scheme (limited) reconstruction (Balagur and Conde 2005) and unlimited fifth-order reconstruction, derived in this article, instead of the second-order reconstruction. Secondly, we introduce a new adaptive version of the central-upwind schemes, in which nonlinear shock and linear contact waves will be treated differently, i.e. fourth-order non-oscillatory scheme (limited) (Balagur and Conde 2005) is applied only near shocks while in the rest of the solution an unlimited fifth-order reconstruction is used. For the fourth-order reconstruction (Balagur and Conde 2005), we used the more general form of the reconstruction presented in

*Corresponding author. Email: dryhhz@yahoo.com

ISSN 1061-8562 print/ISSN 1029-0257 online

DOI: 10.1080/10618561003745464
http://www.informaworld.com

Kurganov and Petrova (2001) to guarantee the non-oscillatory property. The use of unlimited reconstruction may produce some oscillations near contact waves and rarefaction corners, but their amplitude is rather small. These oscillations can be removed by using a nonlinear filter procedure (Engquist *et al.* 1989), applied as a post-processing. Thirdly, we use a more efficient multi-resolution technique (Alves *et al.* 2003) to distinguish between rough and smooth regions. From the numerical results we notice that the size of the multi-resolution coefficient is clearly different that one can distinguish between the shock and the contact discontinuity.

The numerical solution is advanced in time by the strong stability preserving fourth-order accurate five-stage Runge–Kutta solver from Spiteri and Ruuth (2002).

The main advantages of the scheme are:

(1) It is computationally efficient, since limiters are used only near shocks.
(2) It is more accurate and high resolution, since we use a fourth-order non-oscillatory reconstruction near shocks and fifth order reconstruction otherwise.

The rest of the article is organised as follows. Section 2 briefly reviews the semi-discrete central-upwind scheme. In section 3, we describe the fourth-order non-oscillatory and unlimited fifth-order reconstructions. The multi-resolution algorithm is discussed in section 4. In section 5, we present the hybrid scheme. Numerical results for one-dimensional conservation laws are presented in section 6. In section 7, the extension to two-dimensional problems is presented.

2. Semi-discrete central-upwind schemes

We are concerned with the approximations of hyperbolic systems in conservation form

$$u_t + f(u)_x = 0, \quad -\infty < x < \infty, \quad t \geq 0 \tag{1}$$

Subjected to the initial condition

$$u(x,0) = u_0(x) \tag{2}$$

Here $u(x, t)$ is a vector of m components, the conserved variables and $f(u)$ is the physical flux vector. To approximate solution of Equations (1) and (2), we discretise both space and time assuming uniform mesh spacing Δx and Δt, respectively. We denote the spatial grid points by $x_j = j\Delta x$ and the time steps by $t^n = n\Delta t$. Since the solutions of Equations (1) and (2) may develop discontinuities even for smooth initial data, the quantities that will be used on the discrete level are cell averages. The numerical approximation of the cell average in the cell $I_j = \left[x_{j-\frac{1}{2}}, x_{j+\frac{1}{2}}\right]$ centred on x_j at time t^n is denoted by u_j^n:

$$u_j^n = \frac{1}{\Delta x}\int_{x_{j-\frac{1}{2}}}^{x_{j+\frac{1}{2}}} u(x,t^n)dx \tag{3}$$

Assuming that the cell averages at time t^n, u_j^n are known, our goal is to compute the cell averages at the next time step t^{n+1}.We first reconstruct a conservative non-oscillatory piecewise polynomial interpolation $P_j(x)$, $x \in I_j$ from u_j^n, for each cell I_j. The piecewise polynomial reconstructions are, in general, discontinuous at the cell interfaces, $x = x_{j+1/2}$ and therefore their evolution is locally described by the solutions of generalised RPs. The sizes of the corresponding Riemann fans are determined by the right and left sided local speeds of propagation, $\{a_{j+1/2}\}$, which can be estimated by Kurganov *et al.* (2001).

$$\begin{aligned} a^+_{j+1/2} &= \max\left\{\lambda_N\left(\frac{\partial f\left(u^-_{j+1/2}\right)}{\partial u}\right),\ \lambda_N\left(\frac{\partial f\left(u^+_{j+1/2}\right)}{\partial u}\right),\ 0\right\} \\ a^-_{j+1/2} &= \min\left\{\lambda_1\left(\frac{\partial f\left(u^-_{j+1/2}\right)}{\partial u}\right),\ \lambda_1\left(\frac{\partial f\left(u^+_{j+1/2}\right)}{\partial u}\right),\ 0\right\} \end{aligned} \tag{4}$$

with $\lambda_1 < \ldots < \lambda_m$ being the eigenvalues of the Jacobian $\frac{\partial f}{\partial u}$.

Here, $u^+_{i+1/2} = (x_{j+1/2})$, and $u^-_{j+1/2} = P_j(x_{j+1/2})$ are the corresponding right and left values of the piecewise polynomial interpolant $\{P_j(x)\}$ at the cell interface $x = x_{j+1/2}$.

In the nonconvex case, the formula (4) is incorrect if the flux convexity changes near $u^{\pm}_{j+1/2}$, and one should use a more accurate estimate of $\{a^{\pm}_{j+1/2}\}$ there. In this case, the speeds in Equations (4) and (5) can be evaluated exactly:

$$\begin{aligned} a^+_{j+1/2} &= \max_{u\in\left[u^{\min}_{j+1/2},\, u^{\max}_{j+1/2}\right]}\{f'(u), 0\}, \\ a^-_{j+1/2} &= \min_{u\in\left[u^{\min}_{j+1/2},\, u^{\min}_{j+1/2}\right]}\{f'(u), 0\} \end{aligned} \tag{5}$$

where $u^{\min}_{j+1/2} = \min\left\{u^-_{j+1/2}, u^+_{j+1/2}\right\}, u^{\max}_{j+1/2} = \max\left\{u^-_{j+1/2}, u^+_{j+1/2}\right\}$.

For more details, see Kurganov *et al*. (2007).

An exact evolution of the reconstruction is followed by an intermediate piecewise polynomial reconstruction and finally projected back onto the original cells, providing the cell average at the next time step u_j^{n+1}. The semi-discrete central-upwind scheme presented in Kurganov *et al*. (2001) can be written as

$$\frac{d}{dt}u_j(t) = -\frac{1}{\Delta x}\left\{F_{j+\frac{1}{2}} - F_{j-\frac{1}{2}}\right\} = L_j(u). \tag{6}$$

The numerical flux in Equation (6) is given by

$$F_{j+\frac{1}{2}} = \frac{a^+_{j+\frac{1}{2}} \quad f\left(u^-_{j+\frac{1}{2}}\right) - a^-_{j+\frac{1}{2}} \quad f\left(u^+_{j+\frac{1}{2}}\right)}{a^+_{j+\frac{1}{2}} - a^-_{j+\frac{1}{2}}} + \frac{a^+_{j+\frac{1}{2}} \quad a^-_{j+\frac{1}{2}}}{a^+_{j+\frac{1}{2}} - a^-_{j+\frac{1}{2}}}\left[u^+_{j+\frac{1}{2}} - u^-_{j+\frac{1}{2}}\right]. \tag{7}$$

Notice that the accuracy of this scheme is determined by the accuracy of the reconstruction and the ordinary differential equation solver. To integrate Equation (6) forward in time, we use an optimal, strong stability preserving fourth-order accurate five-stage Runge–Kutta solver from Spiteri and Ruuth (2002). To guarantee that no waves interaction occurs during each time step, Δt has to be chosen according to the stability condition

$\mathrm{CFL} \leq 0.5$

Where $\mathrm{CFL} = \max_j\left\{S_j^n \frac{\Delta t}{\Delta x}\right\}$, here S_j^n is the maximum propagation speed in I_j and time level n.

3. Piecewise polynomial reconstruction

As we have mentioned, the piecewise polynomial reconstruction is one of the building blocks of the central-upwind schemes. In this section, we will consider the fourth-order non-oscillatory (limited) reconstruction (Balagur and Conde 2005) and unlimited fifth-order reconstruction, each of which will be applied to the conservative variables component-wise. Therefore, all the variables used in this section are scalar.

3.1. *Fourth-order non-oscillatory reconstruction*

Here, we give a brief description of the fourth-order non-oscillatory reconstruction presented by Balagur and Conde (2005).

Firstly, for a scalar function $u(x)$, we consider the third-order reconstructions

$$\begin{aligned} q_j(x) = u_j^n &- \frac{1}{24}\left[u_{j-1} - 2u_j + u_{j+1}\right] \\ &+ \frac{1}{8}\left[u_{j-1} - u_{j+1} + 10d_j^n\right] \quad \left(\frac{x - x_j}{\Delta x}\right) \\ &+ \frac{1}{2}\left[u_{j-1} - 2u_j + u_{j+1}\right] \quad \left(\frac{x - x_j}{\Delta x}\right)^2 \\ &+ \frac{1}{2}\left[-u_{j-1} + u_{j+1} - 2d_j^n\right] \quad \left(\frac{x - x_j}{\Delta x}\right)^3 \end{aligned} \tag{8}$$

which is conservative and fourth order accurate? Here d_j^n is a slope function.

The reconstruction (8) should satisfy the shape preserving and non-oscillatory properties.

To make Equation (8) satisfy the preserving properties, we have to define a procedure that adequately defines the slopes d_j^n. For this, we use the notation

$$\begin{aligned} dS_j^n &= \frac{2}{3}u_{j+1} - \frac{2}{3}u_{j-1} - \frac{1}{12}u_{j+2} + \frac{1}{12}u_{j-2}, \\ WC_j^n &= u_{j+1} - u_{j-1}, WR_j^n = u_{j+1} - u_j, \\ WC2_j^n &= u_{j+2} - u_{j-2}, dS1_j^n = \frac{WC_j^n}{10}, \\ dS2_j^n &= \frac{1}{2}(WC_j^n - 4WR_j^n) \\ dS3_j^n &= \frac{1}{2}(4WR_j^n - 3WC_j^n), \\ S_j^n = \mathrm{sgn}(WC_j^n),\ C1 &= \frac{\sqrt{15}}{15},\ C2 = \frac{15 - \sqrt{15}}{28}. \end{aligned}$$

Theorem

The reconstruction (8) satisfies the shape preserving properties if d_j^n is defined as:

(A1) If $S_j^n = 0$, then $d_j^n = 0$,

(A2) If $S_j^n \neq 0$ and $(2S_j^n.WC_j^n \geq S_j^n.WC2_j^n)$, then $d_j^n = dS_j^n$

(A3) If $\mathrm{S_j^n} \neq 0$ and $(2\mathrm{S_j^n}.\mathrm{WC_j^n} < \mathrm{S_j^n}.\mathrm{WC2_j^n})$, then the following hold:

(A3.1) if $u_j^n = \frac{u_{j+1}^n + u_{j-1}^n}{2}$ we define

$$d_j^n = \begin{cases} \mathrm{Max}\left[dS1_j^n,\quad dS_j^n\right], & \text{if} \quad S_j^n > 0, \\ \mathrm{Min}\left[dS1_j^n,\quad dS_j^n\right], & \text{if} \quad S_j^n < 0, \end{cases}$$

(A3.2) If $u_j^n \neq \frac{u_{j+1}^n + u_{j-1}^n}{2}$ then the following hold

(A3.2.1) If $\left|WR_j^n - \frac{1}{2}WC_j^n\right| \geq \frac{1}{8}\left|WC2_j^n - 2WC_j^n\right|-$, then

$$d_j^n = \begin{cases} \mathrm{Max}\left[dS2_j^n,\quad dS3_j^n,\ dS_j^n\right], & \text{if} \quad S_j^n > 0, \\ \mathrm{Min}\left[dS2_j^n,\quad dS3_j^n,\ dS_j^n\right], & \text{if} \quad S_j^n < 0, \end{cases}$$

(A3.2.2) If $\left|WR_j^n - \frac{1}{2}WC_j^n\right| < \frac{1}{8}\left|WC2_j^n - 2WC_j^n\right|$, then

$$d_j^n = \begin{cases} WC_j^n - S_j^n.C1.\left|2WR_j^n - WC_j^n\right| & \text{if } \left|\frac{WR_j^n}{WC_j^n} - \frac{1}{2}\right| \le C2 \\ \frac{WC_j^n}{2} & \text{if } \left|\frac{WR_j^n}{WC_j^n} - \frac{1}{2}\right| > C2 \end{cases}.$$

Proof See Balagur and Conde (2005)

To obtain a non-oscillatory reconstruction Balaguer and Conde (2005) consider the modified piecewise reconstruction

$$P_j^n(x) = (1 - \theta_j^n)\, u_j^n + \theta_j^n\, q_j^n(x) \qquad 0 < \theta_j^n < 1 \quad (9)$$

Here we use a more general form proposed by Kurganov and Petrova (2001) which is a combination of q_j^n and the piecewise linear L_j^n, namely

$$P_j^n(x) = (1 - \theta_j^n)\, L_j^n + \theta_j^n\, q_j^n(x) \qquad 0 < \theta_j^n < 1 \quad (10)$$

where

$$L_j^n(x) = u_j^n + w_j^n\,(x - x_j) \quad (11)$$

An appropriate choice of $\{\theta_j^n\}$ and $\{w_j^n\}$ guarantees the non-oscillatory property of the new piecewise reconstruction $P_j^n(x)$ (see Kurganov and Petrova (2001)). We take $\{\theta_j^n\}$ to be

$$\theta_j^n = \begin{cases} \text{Min}\left(\frac{M^n_{j+\frac{1}{2}} - L_j^n\left(x_{j+\frac{1}{2}}\right)}{M_j^n - L_j^n\left(x_{j+\frac{1}{2}}\right)}, \frac{m^n_{j-\frac{1}{2}} - L_j^n\left(x_{j-\frac{1}{2}}\right)}{m_j^n - L_j^n\left(x_{j-\frac{1}{2}}\right)}, 1\right) & \text{if } u_{j-1}^n < u_j^n < u_{j+1}^n \\ \text{Min}\left(\frac{M^n_{j-\frac{1}{2}} - L_j^n\left(x_{j-\frac{1}{2}}\right)}{M_j^n - L_j^n\left(x_{j-\frac{1}{2}}\right)}, \frac{m^n_{j+\frac{1}{2}} - L_j^n\left(x_{j+\frac{1}{2}}\right)}{m_j^n - L_j^n\left(x_{j+\frac{1}{2}}\right)}, 1\right) & \text{if } u_{j-1}^n > u_j^n > u_{j+1}^n \\ 1 & \text{otherwise} \end{cases} \quad (12)$$

where

$$M_j^n = \max\left\{q_j^n(x_{j+\frac{1}{2}}),\ q_j^n(x_{j-\frac{1}{2}})\right\} \text{ and}$$

$$m_j^n = \min\left\{q_j^n(x_{j+\frac{1}{2}}),\ q_j^n(x_{j-\frac{1}{2}})\right\}$$

and

$$M^n_{j\pm\frac{1}{2}} = \max\left\{\frac{1}{2}L_j^n(x_{j\pm\frac{1}{2}}) + L_{j\pm1}^n(x_{j\pm\frac{1}{2}}),\ q_{j\pm1}^n(x_{j\pm\frac{1}{2}})\right\},$$

$$m^n_{j\pm\frac{1}{2}} = \min\left\{\frac{1}{2}L_j^n(x_{j\pm\frac{1}{2}}) + L_{j\pm1}^n(x_{j\pm\frac{1}{2}}),\ q_{j\pm1}^n(x_{j\pm\frac{1}{2}})\right\}$$

Here we take w_j^n as following (Kurganov and Petrova 2001).

$$w_j^n = \min \text{ mod}\left\{\frac{u_j^n - u_{j-1}^n}{\Delta x},\ \frac{u_{j+1}^n - u_j^n}{\Delta x}\right\}. \quad (13)$$

If one sets w_j^n to be zero, then Equations (10)–(13) are reduced to the original reconstruction (Balagur and Conde 2005).

3.2. *Fifth-order reconstruction*

In this subsection, we introduce an unlimited fifth-order reconstruction, realised by the fourth degree polynomial

$$P_j(x) = a_j + b_j\left(\frac{x - x_j}{\Delta x}\right) + c_j\left(\frac{x - x_j}{\Delta x}\right)^2 + d_j\left(\frac{x - x_j}{\Delta x}\right)^3 + e_j\left(\frac{x - x_j}{\Delta x}\right)^4 \quad (14)$$

satisfying fifth-order accuracy and conservation properties. To satisfy these properties the coefficients a_j, b_j, c_j, d_j and e_j should satisfy the following conservation requirements

$$u_{j\pm\ell} = \frac{1}{\Delta x}\int_{x_{j\pm\ell-1/2}}^{x_{j\pm\ell+1/2}} P_j(x,t)dx, \quad \ell = 0, 1, 2. \quad (15)$$

Applying Equation (15) to (14) we obtain the coefficients:

$$a_j(x) = u_j^n + \frac{1}{1920}\left[9u_{j+2} - 116u_{j+1} + 214u_j - 116u_{j-1} + 9u_{j-2}\right] \quad (16)$$

$$b_j(x) = \frac{1}{252}\left[-5u_{j+2} + 136u_{j+1} - 136u_{j-1} + 5u_{j-2}\right] \quad (17)$$

$$c_j(x) = \frac{1}{16}\left[-u_{j+2} + 12u_{j+1} - 22u_j + 12u_{j-1} + 12u_{j-2}\right] \quad (18)$$

$$d_j(x) = \frac{1}{63}\left[u_{j+2} - 2u_{j+1} + 2u_{j-1} - u_{j-2}\right] \quad (19)$$

$$e_j(x) = \frac{1}{24}\left[u_{j+2} - 4u_{j+1} + 6u_j - 4u_{j-1} + u_{j-2}\right]. \quad (20)$$

4. Multi-resolution analysis

The main step in the adaptive scheme proposed in this article is how to distinguish between the smooth region and discontinuities. For this purpose, Harten (1994) introduced a general framework for multi-resolution technique in order to detect the smooth and rough parts of the solution. More recently, Santos *et al.* (2004) and Alves *et al.* (2002, 2003) proposed more efficient multi-resolution algorithms.

In this article, we use the convergent and universally bounded interpolation scheme for the treatment of advection (CUBISTA), Alves *et al.* (2002, 2003), algorithm to distinguish between the smooth parts and discontinuities. This multi-resolution algorithm is found to significantly reduce the computation time and memory requirements as compared to the smoothness indicator (Karni *et al.* 2002).

Consider a set of dyadic grid of the form

$$V^j = \left\{ x_k^j \in R : \; x_k^j = 2^{-j}k, \; k \in Z \right\} \quad (21)$$

where j identifies the resolution level and k the spatial location.

Assume that the function values are known on the grid V^j for $J_{\min} \le j \le J_{\max}$, and we want to extend it to the finer grid V^{j+1}. The even-numbered grid point function values in V^{j+1} are already present in V^j,

$$u_{2k}^{j+1} = u_k^j. \quad (22)$$

The function values in the odd numbered grid points in V^{j+1} are computed using a suitable interpolation from the known even-numbered grid points (present in V^j). The normalised difference between the interpolated value $I^j(u_{2k+1}^{j+1})$, and the real one, u_{2k+1}^{j+1} is called the interpolative error coefficient (or multi-resolution coefficient), d_k^j and is expressed as

$$d_k^j = \left| u_{2k+1}^{j+1} - I^j(u_{2k+1}^{j+1}) \right| / u_{\text{ref}} \quad (23)$$

where

$$u_{\text{ref}} = \max\left(\left| u_{2i+1}^{j+1} \right| \right), \quad i = 0, 1, \ldots 2^j$$

is a reference value of dependent variable.

To calculate the interpolated values, we use the CUBISTA high resolution scheme (Alves *et al.* 2003) as follows:

(1) Compute the face velocity

$$a_{k+\frac{1}{2}} = (a_k^j + a_{k+1}^j)/2$$

(2) Compute the normalised face value $\hat{u}_{k+\frac{1}{2}}$, using the CUBISTA high resolution scheme (Alves *et al.* 2003), the normalised face value is given by

$$\hat{u}_{k+\frac{1}{2}} = \begin{cases} \max\left\{ \left(\frac{u_k^j - u_{k-1}^j}{u_{k+1}^j - u_{k-1}^j} \right), \min\left(\frac{7}{4}\frac{u_k^j - u_{k-1}^j}{u_{k+1}^j - u_{k-1}^j}, \; \frac{3}{4}\frac{u_k^j - u_{k-1}^j}{u_{k+1}^j - u_{k-1}^j} + \frac{3}{8}, \; \frac{3}{4} + \frac{1}{4}\frac{u_k^j - u_{k-1}^j}{u_{k+1}^j - u_{k-1}^j} \right) \right\}, \\ \qquad\qquad \text{if } a_{k+\frac{1}{2}} \ge 0 \\ \max\left\{ \left(\frac{u_{k+1}^j - u_{k+2}^j}{u_k^j - u_{k+2}^j} \right), \min\left(\frac{7}{4}\frac{u_{k+1}^j - u_{k+2}^j}{u_k^j - u_{k+2}^j}, \; \frac{3}{4}\frac{u_{k+1}^j - u_{k+2}^j}{u_k^j - u_{k+2}^j} + \frac{3}{8}, \; \frac{3}{4} + \frac{1}{4}\frac{u_{k+1}^j - u_{k+2}^j}{u_k^j - u_{k+2}^j} \right) \right\}, \\ \qquad\qquad \text{if } a_{k+\frac{1}{2}} < 0 \end{cases} \quad (24)$$

(3) Calculate the interpolated value:

$$I^j(u_{2k+1}^{j+1}) = \begin{cases} u_{k-1}^j + \hat{u}_{k+\frac{1}{2}}^j (u_{k+1}^j - u_{k-1}^j), & \text{if } a_{k+\frac{1}{2}} \ge 0 \\ u_{k+2}^j + \hat{u}_{k+\frac{1}{2}}^j (u_k^j - u_{k+2}^j), & \text{if } a_{k+\frac{1}{2}} < 0. \end{cases} \quad (25)$$

The multi-resolution coefficients $\{d_k^j\}$ are used to generate a shock detection mechanism where an unlimited fifth-order reconstruction is switched to non-oscillatory fourth-order reconstruction whenever d_k^j is larger than a tolerance parameter ε.

The maximum and minimum level of resolution should be specified by the user to avoid coalescence in problematic region (here we use $J_{\max} = 12$ and $J_{\min} = 4$).

***Remark* 1**

We must add all the grid points necessary for the calculation of the interpolative error coefficients at the next resolution level. This step is dependent on the interpolative scheme used to evaluate $\tilde{I}^j(u^{j+1}_{2k+1})$. Here we use the high resolution for which the calculation of d^j_k implies the presence of grid points at locations x^j_{k-1}, x^j_k, x^j_{k+1} and x^j_{k+2}. (For more details see Alves *et al.* (2003) and Santos *et al.* (2004).)

***Remark* 2**

It is important here to note that the superscript (j) here denotes the number of the resolution level while in the rest of the article it denotes the time level.

4.1. Shock adaptation algorithm

In this section, we derive the order of the interpolative error (multi-resolution) coefficient (MR) for systems of conservation laws. In fact, since the solutions of the nonlinear conservation laws are in general nonsmooth, standard method of convergence rate analysis, based on Taylor expansions are invalid, therefore we derive the order of MR numerically.

We compute the order of the MR for system of Euler equations of gas dynamics

$$U_t + F(U)_x = 0, \tag{26}$$

where $U=(\rho,\rho u,E)^T$ and $F(U)=(\rho u,\rho u^2+P,u(E+P))^T$, here ρ is the density, u is the velocity, P is the pressure, $E = \frac{1}{2}\rho u^2 + \frac{P}{(\gamma-1)}$ is the total energy and γ is the ratio of specific heats, taken as 1.4 here.

The initial data correspond to the shock tube problem proposed by Sod (1987).

$$\begin{gathered}\rho_{\mathrm{L}} = 1.0, \quad \rho_{\mathrm{R}} = 0.125, \quad u_{\mathrm{L}} = u_{\mathrm{R}} = 0.0,\\ P_{\mathrm{L}} = 1.0, \quad P_{\mathrm{R}} = 0.1, \quad \gamma = 1.4\end{gathered} \tag{27}$$

on a tube of unit length. The diaphragm is at $x_0 = 0.5$, subscripts L and R denote values to the left and right of x_0. The numerical solutions are displayed after $t = 0.16$, with $N = 2^7 + 1$ and CFL $= 0.4$.

Figures 1 and 2 show the computed results using AD4SC and AD4S (AD4SC: in which we use the limited fourth-order reconstruction near discontinuities (shocks and contact) and the unlimited fifth-order reconstruction in the smooth regions and AD4S: in which the limited fourth-order reconstruction is used near shock waves only while in the rest of the computational domain, an unlimited fifth-order reconstruction is used) schemes, respectively.

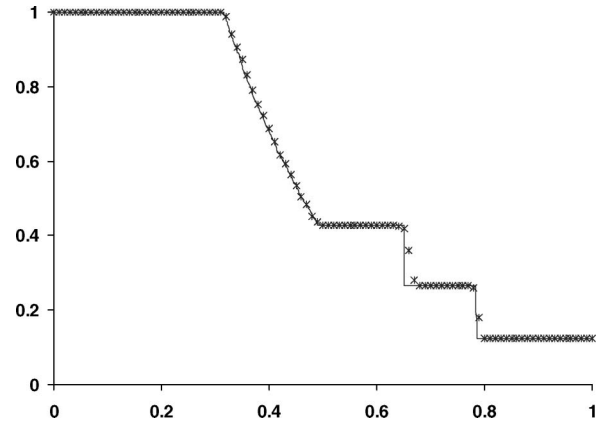

Figure 1. Solution of Equation (26) with (27) using AD4SC scheme.

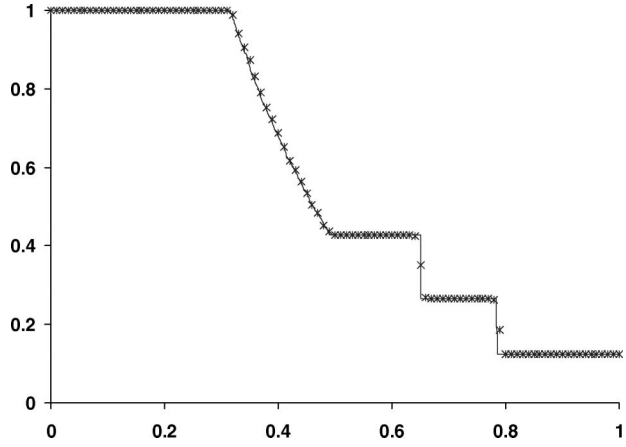

Figure 2. Solution of Equation (26) with (27) using AD4S scheme.

In Figure 3, we show the values of the multi-resolution coefficients. We note that the difference in size of the MR between the shock and contact discontinuities shows the ability of our MR to distinguish between the shock and contact discontinuities.

The convergence rates of the MR, measured in the smooth part of the rarefaction wave, near the contact discontinuity and near the shock are shown in Tables 1–3, respectively. From the tables, we note that the convergence rate in smooth sub-region appears to be $0(\Delta x)^3$ and only $0(\Delta x)$ near the shock while the convergence rate in the neighbourhood of the linear contact is between $0(\Delta x)$ and $0(\Delta x)^2$.

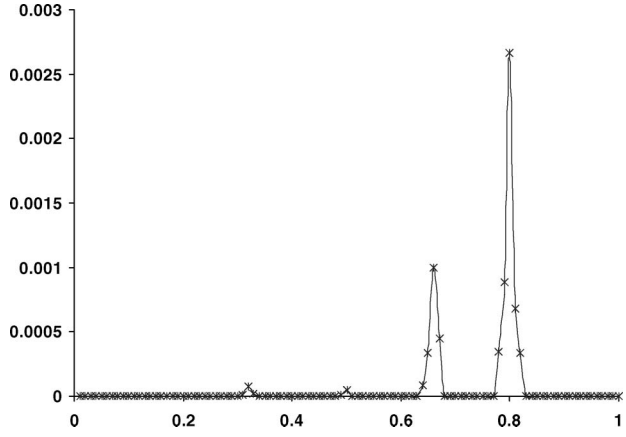

Figure 3. Multi-resolution coefficient of Equation (26) with (27).

Table 1. Convergence rates for MR for shock tube problem in the smooth sub-region [0.35,0.45].

N	L^1 error	L^1 order
64	8.182E-6	
128	7.836E-7	3.38
256	8.047E-8	3.28
512	3.786E-9	4.41
1024	3.268E-10	3.53
2048	4.096E-11	2.996

Table 2. Convergence rates for MR for shock tube problem near contact of discontinuity [0.6,0.7].

N	L^1 error	L^1 order
64	3.081E-3	
128	1.196E-3	1.37
256	4.986E-4	1.26
512	2.015E-4	1.31
1024	7.931E-5	1.35
2048	3.088E-5	1.36

Table 3. Convergence rates for MR for shock tube problem near the shock [0.75, 85].

N	L^1 error	L^1 order
64	6.671E-2	
128	2.912E-2	1.196
256	1.379E-2	1.08
512	6.814E-3	1.02
1024	3.337E-3	1.03
2048	1.635E-3	1.03

Therefore, we get

$$\|MR\|_1 = \begin{cases} O(\Delta x), & \text{near shocks} \\ O(\Delta x)^{\alpha}, & \text{near contact discontinuities,} \\ & \alpha \in [1,2] \\ O((\Delta x)^3), & \text{in the smooth region} \end{cases} \tag{28}$$

Similar to the procedure in Constantin and Kurganov (2006) we conclude the following condition

$$\begin{cases} \text{if } |MR| > K\,\|MR\|_1, & \text{near shocks} \\ \text{otherwise} & \text{out of shock region} \end{cases} \tag{29}$$

where K is the adaptation constant to be chosen. In the numerical experiments, we note that the optimal interval of K is [5,10]. For any value inside this interval the numerical results are the same. Here we take $K = 5$.

Remark

We should know that the MR coefficient can distinguish easily between smooth region and non-smooth regions (both shock and contact discontinuities) by considering one tolerance parameter as the following

$$\begin{cases} \text{if } |MR| > \varepsilon & \text{near discontinuities} \\ \text{otherwise} & \text{smooth region} \end{cases} \tag{30}$$

where ε is tolerance parameter defined by the user.

Remark

The tolerance ε determines the dynamic activation of the fourth-order non-oscillatory reconstruction with limiters and the unlimited fifth-order reconstruction along the various sub-domains of the adaptive scheme. While too small a value of ε activates the more expensive non-oscillatory method at sub-domains where the solution is smooth or contact discontinuities, a larger value of ε activates the unlimited method at sub-domain with low spatial resolution, generating oscillations. Actually, there is a relation between ε and MR order. High MR order values decrease the size of ε one needs to choose, since high frequencies are less mistaken by gradient jumps. For most of the flows with shock that were tested (some of them are presented here and others are not), the value of $\varepsilon = 10^{-4}$ yielded a good balance between computational speed and accuracy of the numerical solutions.

5. Scheme adaptation

In this section, we introduce our adaptive central-upwind scheme. In this particular context, we define the scheme as a grid-based adaptive method in which the choice of the numerical scheme is determined by the smoothness of the solution at each grid point. This can be done by the multi-resolution procedure, mentioned in section 4.

The implementation of the adaptive scheme is summarised in the following steps:

(1) Compute the multi-resolution coefficients d_k^j for $J_{\min} \leq j \leq J_{\max} - 1$ from Equation (23) at each grid point.
(2) A grid point is flagged as smooth or non-smooth according to Equation (29).
(3) Once the flags are set, a number of neighbouring points around each flagged point x_i, depending on the number of the ghost points needed for a given order of the scheme, are also flagged to 1 or 2.
(4) For the points flagged 2 (shock) we compute the numerical flux $F_{j+\frac{1}{2}}$ (Equation (7)) with the fourth-order non-oscillatory reconstruction (9) with the limiters (Equation (12)).
(5) Otherwise (smooth and contact), we compute the numerical flux $F_{j+\frac{1}{2}}$ (Equation (7)) with the unlimited fifth-order reconstruction (14) with the coefficients (Equations (16)–(20)).
(6) Knowing the numerical flux $F_{j+\frac{1}{2}}$, in the last steps, solve the ODE (6) by using fourth-order SSP Runge-Kutta scheme to get u_j^{n+1}.
(7) The use of unlimited reconstruction may result in some oscillations near contact discontinuities and rarefaction corners. These oscillations can be removed by the help of a nonlinear filter, proposed by Engquist *et al*. (1989), applied as a post-processing.

Remark

The multi-Resolution analysis is applied only once at the beginning of the Runge-Kutta time stepping scheme.

6. Numerical results

In this section, we present numerical solutions for the system of Euler equations of gas dynamics (26).

We compare the following schemes:

(1) AD4SC: in which we use the limited fourth-order reconstruction near discontinuities (shocks and contact) and the unlimited fifth-order reconstruction in the smooth regions.
(2) AD4S: in which the limited fourth-order reconstruction is used near shock waves only while in the rest of the computational domain, an unlimited fifth-order reconstruction is used.

In all examples we use a uniform mesh, N denotes the number of cells and exact solution is shown by solid line and the numerical solutions are shown by symbols and CFL = 0.4. Also, we take $\varepsilon = 10^{-4}$ as a tolerance in Equation (30). Here we use the nonlinear filtered proposed by Engquist *et al*. (1989).

6.1. *Lax problem*

We solve the Lax problem (Bryson and Levy 2006) for Euler Equations (31) and the initial data:

$$\begin{aligned} &(\rho_L, u_L, P_L) = (0.445,\ 0.311,\ 3.5626) \\ &\text{and} \quad (\rho_R, u_R, P_R) = (0.5,\ 0.0,\ 5.71). \end{aligned} \tag{31}$$

Separated by a discontinuity at $x = 0.5$, the computational domain is taken as the unit interval [0,1] and the results at $t = 0.16$ with $2^7 + 1$ grid points. Figure 4 shows the multi-resolution coefficients and the threshold. From the figure we can easily distinguish between shocks and contact discontinuities. Figure 5 shows the results using AD4S without filter and Figures 6 and 7 depict the graphical results of AD4SC and AD4S schemes, respectively. We observe the clear

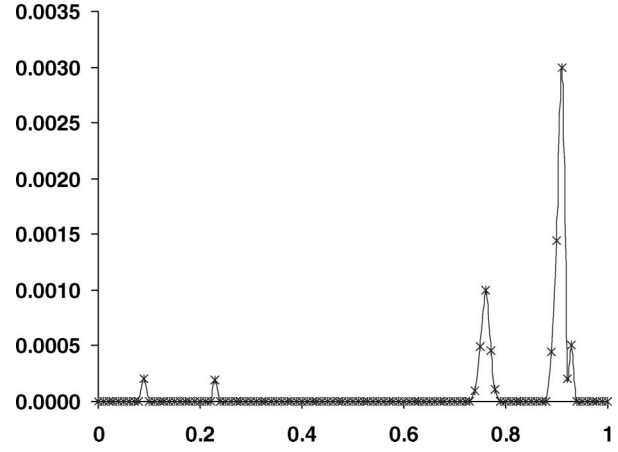

Figure 4. Multi-resolution coefficient of Equation (31).

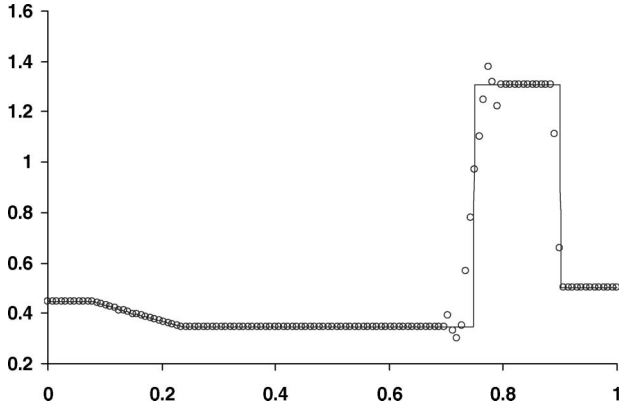

Figure 5. Solution of Equation (31) using AD4S without filter.

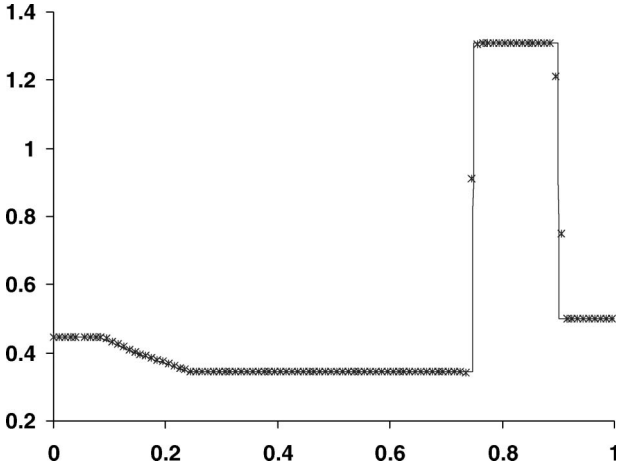

Figure 6. Solution of Equation (31) using AD4SC scheme.

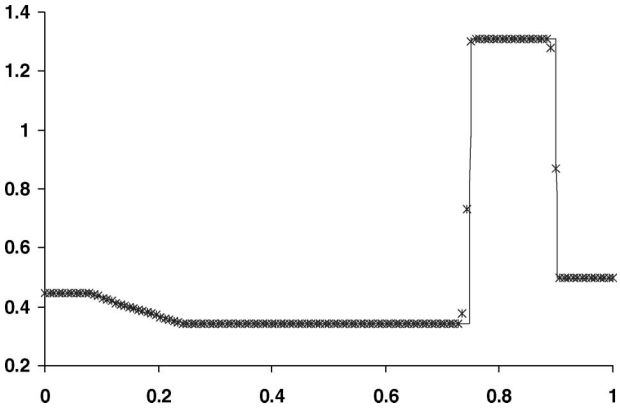

Figure 7. Solution of Equation (31) using AD4S scheme.

improvements in accuracy as we move from AD4SC to AD4S scheme. Note that the contact is well resolved by AD4S scheme. We note also here that the numerical results of the adaptive schemes are more accurate than those obtained by the non-oscillatory scheme (Balagur and Conde 2005).

6.2. *Three discontinuities travelling to the right*

We consider the test problem concerning three discontinuities travelling to the right in a domain [0,1], governed by Euler equations (31) with the initial data: (Toro 1999)

$$(\rho, u, P) = \begin{cases} (5.99924, 19.5975, 460.894), & 0 \le x \le 0.4 \\ (5.99242, -6.19633, 46.095), & 0.4 < x \le 1.0 \end{cases}, \quad \gamma = 1.4 \tag{32}$$

The numerical solutions are obtained at $t = 0.035$ with $N = 2^7 + 1$. Figure 8 illustrates the multi-resolution coefficients. Figure 9 shows the results of AD4SC scheme. The shocks are captured with two points and the contact with two points. Figure 10 shows the performance of the adaptive scheme AD4S. As seen in the figure, the application of the AD4S scheme leads to an improved resolution of the contact wave, since no limiters are applied in its vicinity, where the value of multi-resolution coefficient is much smaller than ones at the shocks (see Figure 8).

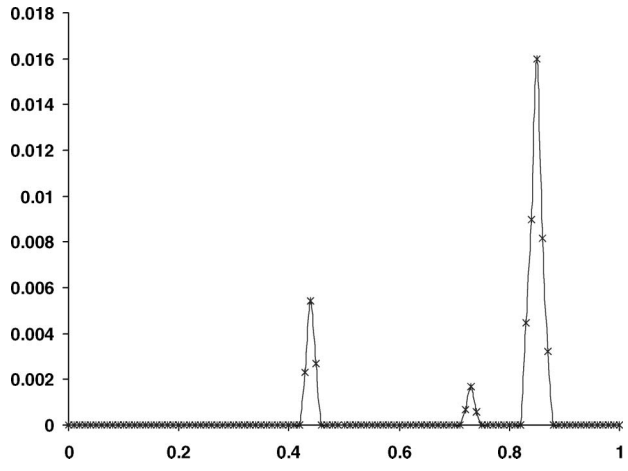

Figure 8. Multi-resolution coefficient of Equation (32).

6.3. *Shock/turbulence interaction problem*

To show the advantages of our scheme, we will solve a problem with a rich smooth structure and a shock wave. A typical example for this is the problem of shock interaction with entropy waves (Bryson and Levy 2006).

We solve the Euler equations (31) with a moving Mach = 3 shock interacting with sine waves in density, i.e. initially (Bryson and Levy 2006)

$$\begin{aligned} (\rho_L, u_L, P_L) &= (3.857143, 2.629369, 10.3333), \quad \text{for } x \le 0.1 \\ (\rho_R, u_R, P_R) &= (1 + 0.2\sin 50x, 0, 1), \quad \text{for } x > 0.1 \end{aligned} \tag{33}$$

The flow contains physical oscillations which have to be resolved by the numerical method. We compute the solution at $t = 0.18$. Figure 11 illustrates the multi-resolution coefficients. Figures 12 and 13 show the computed density by AD4SC and AD4S schemes against the reference solution, which is a converged

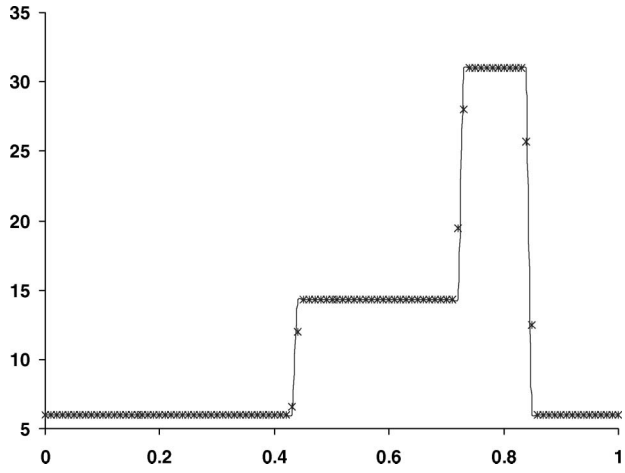

Figure 9. Solution of Equation (32) using AD4SC scheme.

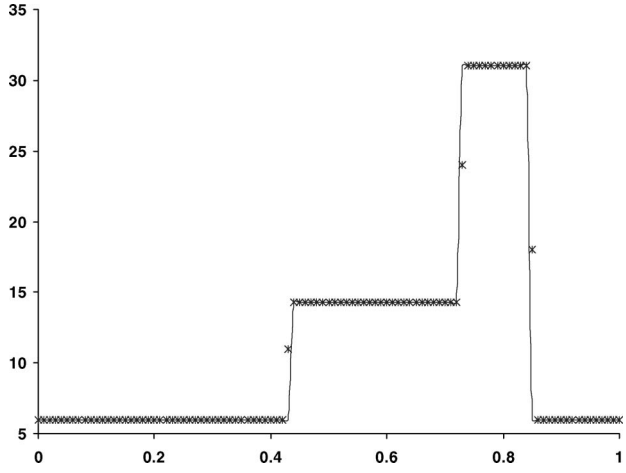

Figure 10. Solution of Equation (32) using AD4S scheme.

solution computed by the fifth-order finite difference WENO scheme (Qiu and Shu 2002) with 2000 grid points. Here we use $2^8 + 1$ grid points. We observe the clear improvements in accuracy as we move from AD4SC scheme to AD4S scheme. The AD4S scheme produces more accurate solutions, which are very close to the reference solution.

Remark

If we compare these results with the results obtained by the high-order hybrid central-WENO scheme of Bruno and Don (2007), we notice that the results here provide a more accurate solution (see Figure 3 in Bruno and Don (2007)).

6.4. Blast wave problem

The blast problem introduced by Woodward and Colella (1984) is severe test problem and therefore a good problem to test the robustness of numerical schemes. This problem has the initial condition consisting of three states:

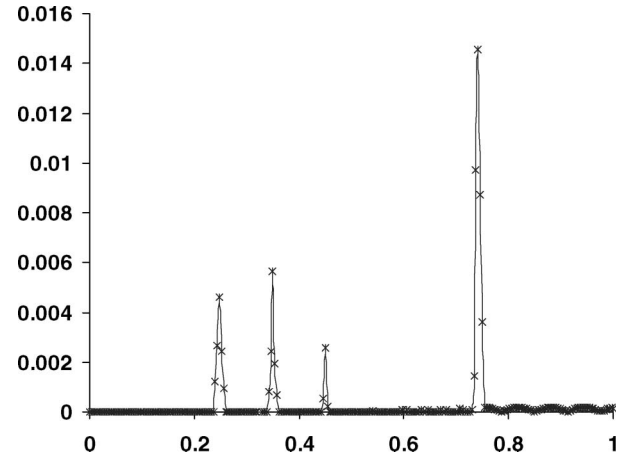

Figure 11. Multi-resolution coefficient of Equation (33).

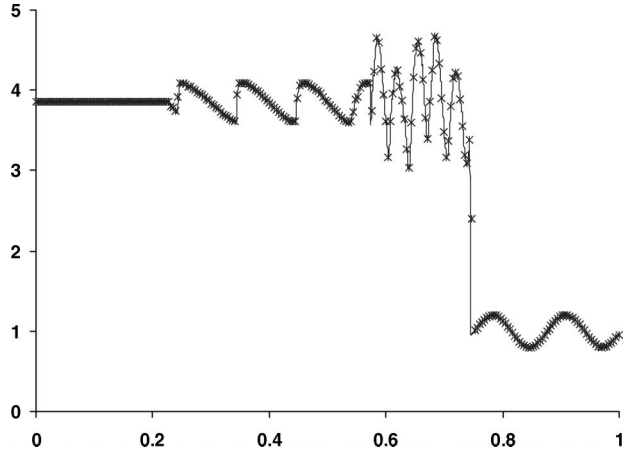

Figure 12. Solution of Equation (33) using AD4SC scheme.

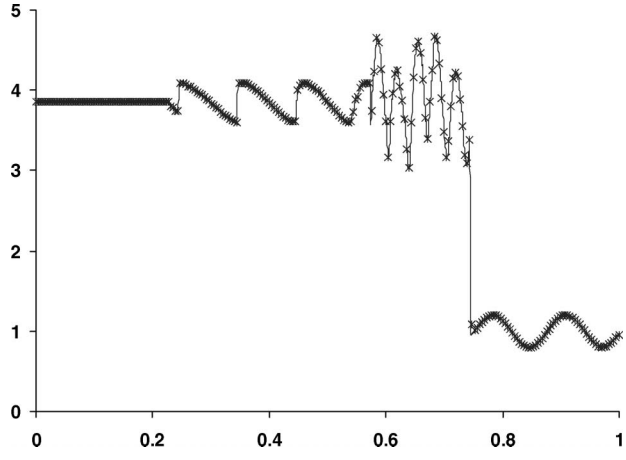

Figure 13. Solution of Equation (33) using AD4S scheme.

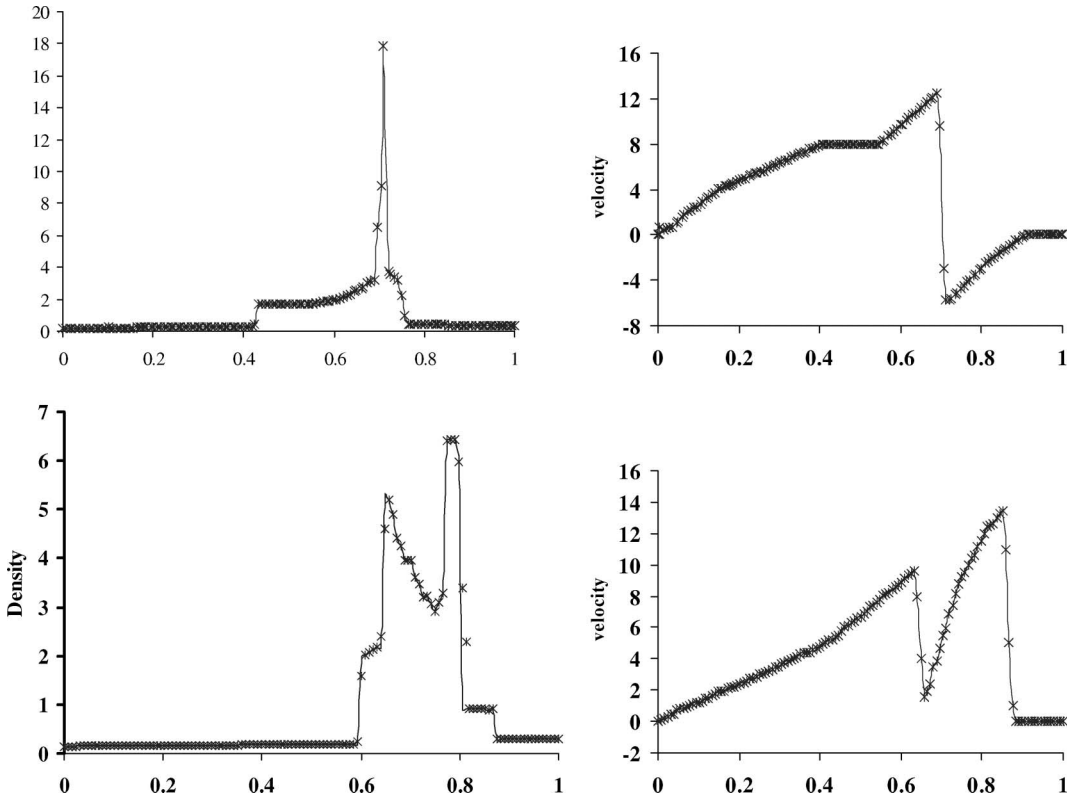

Figure 14. Velocity and density of blast problem (34) using AD4S at $t = 0.028$ (up) and $t = 0.038$ (down).

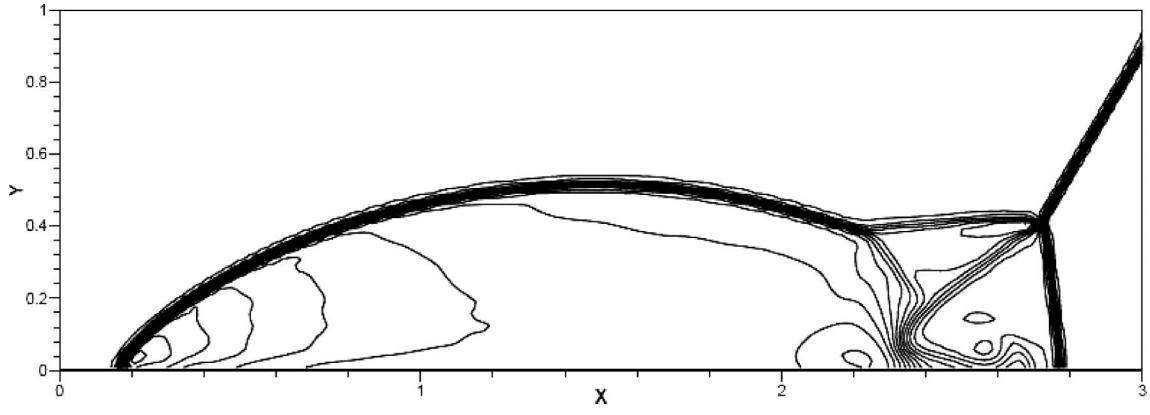

Figure 15. Double Mach reflection problem for the AD4S scheme, meshes of 240 × 60.

$$U(x,0) = \begin{cases} (\rho_L, u_L, P_L) = (1,0,1000), & x < 0.1 \\ (\rho_M, u_M, P_M) = (1,0,0.01) & 0.1 < x < 0.9 \\ (\rho_R, u_R, P_R) = (1,0,100) & x > 0.9 \end{cases}. \tag{34}$$

With $\gamma = 1.4$, boundary conditions are reflective. The solution of this problem contains the propagation of strong shock waves into low pressure regions, the collision of strong shock waves and interaction of shock waves and rarefactions.

We display the numerical results of the density and velocity of this complex problem in Figure 14. The results are with $N = 2^7 + 1$ cells at time $t = 0.028$ and $t = 0.038$ and we get the reference solution from fifth-order WENO (Toro 1999) scheme on 4000 cells.

Figure 14 shows the density and velocity obtained by AD4S scheme. It is noticed that the AD4S scheme is

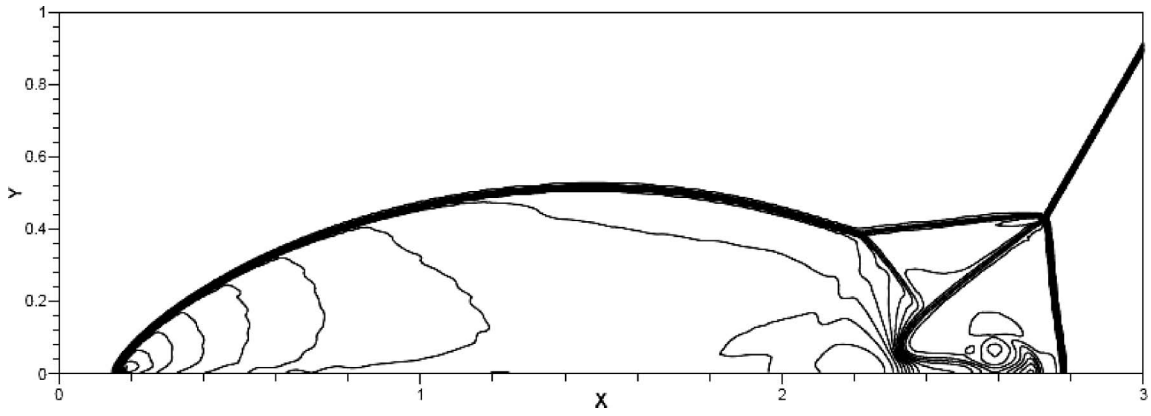

Figure 16. Double Mach reflection problem for AD4S scheme, meshes of 480 × 120.

able to obtain such sharp resolution of the complex double blast problem.

7. Extension to multidimensional problems

The present schemes can be applied to multidimensional problems using a dimension-by-dimension approach. As an example, we consider the two-dimensional, Euler equations

$$U_t + [F(U)]_x + [G(U)]_y = 0 \tag{35}$$

where

$$U = (\rho, \rho u, \rho v, E)^T,$$
$$F(U) = (\rho u, P + \rho u^2, \rho uv, u(P + E))^T,$$
$$G(U) = (\rho v, \rho uv, P + \rho v^2, v(P + E))^T.$$

7.1. Double Mach reflection problem

The governing equation for this problem is the two-dimensional Euler equation (35). The computational domain is $[0,4] \times [0,1]$. The reflecting wall lies at the bottom of the computational domain starting from $x = \frac{1}{6}$. Initially, a right moving Mach 10 shock is positioned at $(x, y) = (\frac{1}{6}, 0)$ and makes a 60° angle with the x-axis. For the bottom boundary, the exact post-shock condition is imposed from $x = 0$ to $x = \frac{1}{6}$ and a reflective boundary condition is used for the rest of the x-axis. At the top boundary of the computational domain, the data are set to describe the exact motion of the Mach 10 shock; see Sod (1987) for a detailed discussion of this problem.

Figures 15 and 16 show the computed density by AD4S scheme on the 240 × 60 and 480 × 120 cells. We observe that the scheme produces the flow pattern generally accepted in the present literature (Woodward and Colella 1984) as correct. All discontinuities are well resolved and correctly positioned.

References

Alves, M.A., *et al*., 2002. Adaptive multi-resolution approach for solution of hyperbolic PDEs. *Computer Methods in Applied Mechanics and Engineering*, 191, 3909–3928.

Alves, M.A., Oliveira, P.J., and Pinho, F.T., 2003. A convergent and universally bounded interpolation scheme for the treatment of advection. *International Journal for Numerical Methods in Fluids*, 41, 47–75.

Balagur, A. and Conde, C., 2005. Fourth order non-oscillatory upwind and central schemes for hyperbolic conservation laws. *SIAM Journal on Numerical Analysis*, 43 (2), 455–473.

Bruno, C. and Don, W.S., 2007. High order hybrid central-WENO finite difference scheme for conservation laws. *Journal of Computational and Applied Mathematics*, 204 (2), 209–218.

Bryson, S. and Levy, D., 2006. On the Total Variation of high-order semi-discrete central schemes for conservation laws. *Journal of Scientific Computing*, 27, 163–175.

Constantin, L.A. and Kurganov, A., 2006. Adaptive central-upwind schemes for hyperbolic systems of conservation laws. *In*: *Hyperbolic problems: theory, numerics, applications*. Osaka, Japan: Yokohama Publishers, 95–103.

Engquist, B., Lotstedt, P., and Sjogreen, B., 1989. Nonlinear filters for efficient shock computation. *Mathematics of Computation*, 52, 509–537.

Harten, A., 1994. Adaptive multi-resolution schemes for shock computations. *Journal of Computational Physics*, 115, 319–338.

Karni, S. and Kurganov, A., 2005. Local error analysis for approximate solutions of hyperbolic conservation laws. *Advances in Computational Mathematics*, 22, 79–99.

Karni, S., Kurganov, A., and Petrova, G., 2002. A smoothness indicator for adaptive algorithms for hyperbolic systems. *Journal of Computational Physics*, 178, 323–341.

Kurganov, A., Noelle, S., and Petrova, G., 2001. Semi-discrete central-upwind schemes for hyperbolic conservation laws and Hamilton-Jacobi equations. *SIAM Journal on Scientific Computing*, 23, 707–740.

Kurganov, A. and Petrova, G., 2001. A third-order semi-discrete genuinely multidimensional central scheme for hyperbolic conservation laws and related problems. *Numerische Mathematik*, 88, 683–729.

Kurganov, A., Petrova, G., and Popov, B., 2007. Adaptive semi-discrete central-upwind schemes for nonconvex hyperbolic conservation laws. *SIAM Journal on Scientific Computing*, 29, 2381–2401.

Qiu, J. and Shu, C.-W., 2002. On the construction, comparison, and local characteristic decomposition for the high order central WENO schemes. *Journal of Computational Physics*, 183, 187–209.

Santos, J.C., *et al*., 2004. Adaptive multi-resolution approach for two dimensional PDEs. *Computer Methods in Applied Mechanics and Engineering*, 193, 405–425.

Sod, G., 1987. A survey of several finite difference methods for systems of nonlinear hyperbolic conservation laws. *Journal of Computational Physics*, 27, 1–31.

Spiteri, R.J. and Ruuth, S.J., 2002. A new class of optimal high-order strong-stability-preserving time discretization methods. *SIAM Journal on Numerical Analysis*, 40 (2), 469–491.

Toro, E.F., 1999. *Riemann solvers and numerical methods for fluid dynamics*. 2nd ed. Berlin: Springer-Verlag.

Woodward, P. and Colella, P., 1984. The numerical solution of two dimensional fluid flow with strong waves. *Journal of Computational Physics*, 54, 115–173.